GA–A27860

H-MODE TRANSITIONS AND LIMIT CYCLE OSCILLATIONS FROM MEAN FIELD TRANSPORT EQUATIONS

by

G.M. STAEBLER and R.J. GROEBNER

AUGUST 2014

GENERAL ATOMICS

DISCLAIMER

GA–A27860

H-MODE TRANSITIONS AND LIMIT CYCLE OSCILLATIONS FROM MEAN FIELD TRANSPORT EQUATIONS

by
G.M. STAEBLER and R.J. GROEBNER

This is a preprint of an invited paper to be presented at the Forty-First European Physical Society Conf. on Plasma Physics, June 23–27, 2014 in Berlin, Germany and to be published in *Plasma Phys. and Controlled Fusion.*

Work supported by
the U.S. Department of Energy under
DE-FG02-95ER54309 and DE-FC02-04ER54698

GENERAL ATOMICS PROJECT 03726
AUGUST 2014

Abstract

The mean field toroidal and parallel momentum transport equations will be shown to admit both one-step transitions to suppressed transport (L/H) and limit cycle oscillations (LCO). Both types of transitions are driven by the suppression of turbulence by the mean field ExB velocity shear. Using experimental data to evaluate the coefficients of a reduced transport model, the observed frequency of the LCO can be matched. The increase in the H-mode power threshold above and below a minimum density agrees with the trends in the model. Both leading and lagging phase relations between the turbulent density fluctuation amplitude and the ExB velocity shear can occur depending on the evolution of the linear growth rate of the turbulence. The transport solutions match the initial phase of the L/H transition where the poloidal and ExB velocities are observed to change, and the density fluctuations drop, faster than the diamagnetic velocity.

1. Introduction

The focus of this paper is to show that the mean field momentum transport equations have both one-step L/H transitions and limit cycle oscillations (LCO) or dithering transitions. A simplified model, based on the properties of gyrokinetic turbulence, is used to demonstrate the two types of solutions. The data from the L-mode phase of a DIII-D [1] tokamak discharge 140426 at 1265 ms at the major radius of R=2.265 m (toroidal flux surface $\rho = 0.98$) prior to the LCO will be used to evaluate the model parameters as much as is possible. This will be referred to as the reference data. A summary of the data used is given in table 1. Extensive turbulence measurements during the LCO phase have been made for this discharge and similar ones and published in reference [2]. The calculated velocities and density fluctuation amplitudes in this paper can be compared with the measurements in reference [2] by the reader. The reasonable agreement with the data achieved with such a simple model verifies that the mean field transport equations contain the right physics to simulate the LCO and L/H transitions. The simple model also shows trends in qualitative agreement with the power threshold scaling with density. Oscillating solutions of the toroidal and parallel (or poloidal) momentum transport solutions have been observed in previous phenomenological modeling of internal transport barrier dynamics [3,4]. Analysis of the LCO solutions in this paper identify the cause of the oscillations. It is well established that ExB velocity shear supresses turbulence and improves transport in all channels: energy, particle, momentum [5]. One outstanding puzzle has been the observation that the velocity of the plasma changes first and faster than the pressure or density profiles [6]. This is known as the L/H "trigger". In this paper it will be shown that the mean field momentum transport provides this fast change in velocity that triggers the suppressed turbulence. Particle and energy transport would also be improved but will not be included in the modeling in order to clearly demonstrate that the oscillation is due to momentum transport physics. This work establishes that the mean field transport equations can, in principle be a predictive theory of the L/H transition, given an accurate model of the turbulence driven fluxes in all channels. There are many physical effects that can be important in momentum transport that will not be considered in this work. In particular, the ion orbit loss cone at the separatrix [7,8] and the reduction of the poloidal damping term at high mach number [7,8] are neglected. The turbulent momentum transport and poloidal damping by Coulomb collisions are assumed to be the dominant contributions.

Table 1
Local data for DIII-D discharge 140426 at 1265 ms and ρ=0.98

n_e	T_e	T_i	L_{ne}	L_{Te}	L_{Ti}	χ_{tot}	c_s
$1.7 \times 10^{19}/m^3$	64 eV	150 eV	9.26 cm	1.37 cm	4.16 cm	10.3 m^2/s	5.4×10^4 m/s
R	**r**	R_{ref}	B_{ref}	**q**	B_z	B_{unit}	ρ_s
2.265 m	58.0 cm	1.68 m	-2.01 T	4.5	-0.34 T	-2.93 T	0.039 cm
c_{par}	c_{per}	c_{tor}	ν_{exch}	ν_i	ν_{pol}	Ω_s	ν_i^*
0.502	0.663	1.063	684/s	4790/s	632/s	6.6×10^7/s	4.5

2. Mean Fields and Fluctuations

It is important to verify that there is sufficient time scale separation to define the mean fields and fluctuations. The mean fields are defined as an ensemble average of the total fields involving both space and time averages [9]. For example the ensemble average $\langle\langle A \rangle\rangle$ of some field A (i.e. electric, magnetic or particle distribution) could be a magnetic flux surface average $\langle A \rangle$ followed by a moving boxcar time and radius average with averaging time τ and length L. The length and time scales of the averaging are chosen to give separation $A = A_0 + \tilde{A}$ between the fluctuating $\tilde{A}$ and mean fields A_0. The fluctuations are annihilated by the ensemble average $\langle\langle \tilde{A} \rangle\rangle = 0$. In general, the time average has to be longer than the decorrelation time of the turbulence. For the experimental conditions of the reference L-mode plasma prior to the onset of the LCO (table 1) the measured decorrelation time of the density fluctuations was 2 μs [2]. The LCO period for the reference data was 625 μs and the fastest timescale (fluctuation drop) of the L/H transition is about 100 μs [10]. The solutions to the momentum transport equations will be shown to reproduce both the LCO and L/H timescales so, for the purpose of separating fluctuations and mean fields, a 100 μs time average is optimal. This is 50 times the decorrelation time so there is enough time separation to average out the fluctuations. The Doppler shift velocity of the turbulence measured with Doppler backscatter (DBS) is averaged over 100 μs [2]. Thus, the Doppler shift velocity measured by DBS should be considered the mean field ExB velocity contribution that can be compared with the transport solution for the ExB velocity. The term zonal flows has often been used in the literature to refer to the ExB velocity due to an axisymmetric radial electric field without separation of timescales. Using the ensemble average separates *zonal fluctuations* from the mean field ExB velocity. The zonal fluctuations, are governed by the gyrokinetic equation on the decorrelation timescale that is far faster than the observed LCO oscillations and are filtered out of the time average DBS data.

The separation of faster fluctuations from slower mean fields is the basis for traditional ordering expansions. Systematic derivations of the gyrokinetic equation [9] for the fluctuations and transport equations for the mean fields, including both turbulence driven fluxes and Coulomb collision terms, have been published [11–13]. Because of the conservation of total momentum (summed over all species a = ions, electrons) by the coulomb collision operator there are no Coulomb force terms in either the total toroidal or parallel momentum transport equations [14]. Hence, the parallel momentum balance equation will be the most susceptible to modification by turbulence from the neoclassical result [13]. The total toroidal and parallel to the magnetic field $\left(\vec{B}\right)$ momentum transport equations in the right handed toroidal coordinates (R,φ,Z) averaged over a magnetic flux surface are [13]

$$\sum_a \left[\frac{\partial}{\partial t} \left\langle m_a n_a R^2 \vec{\nabla}\varphi \cdot \vec{u}_a \right\rangle + \left\langle R^2 \vec{\nabla}\varphi \cdot \left(\vec{\nabla} \cdot \vec{\vec{\Pi}}_a \right) \right\rangle \right] = \sum_a \left\langle R^2 \vec{\nabla}\varphi \cdot \vec{S}_a \right\rangle \quad , \tag{1}$$

$$\sum_a \left[\frac{\partial}{\partial t} \left\langle m_a n_a \vec{B} \cdot \vec{u}_a \right\rangle + \left\langle \vec{B} \cdot \left(\vec{\nabla} \cdot \vec{\vec{\Pi}}_a \right) \right\rangle \right] = \sum_a \left\langle \vec{B} \cdot \vec{S}_a \right\rangle \quad . \tag{2}$$

The mean velocity is $\left(\vec{u}_a\right)$, the mean density is n_a and the mass is m_a. The external momentum sources are $\left(\vec{S}_a\right)$. There are, in general, turbulent and collisional contributions to the stress tensor $\left(\vec{\vec{\Pi}}_a = \vec{\vec{\Pi}}_a^{turb} + \vec{\vec{\Pi}}_a^{col}\right)$. The importance of the parallel momentum transport equation for H-mode was first emphasized by Rozhanski and Tendler [15].

The 1st order in ρ_s/L mean field species velocities are within flux surfaces and incompressible [13]. For low mach number they can be written in terms of two flux functions $\left(K_a, \Omega_a\right)$: $\vec{u}_a = \vec{B} K_a + R^2 \vec{\nabla}\varphi \Omega_a$. The flux surface average velocities are

$$\left\langle R^2 \vec{\nabla}\varphi \cdot \vec{u}_a \right\rangle \Big/ R_{ref} = c_{per} u_{a,pol} + c_{tor} \left(u_{ExB} + u_{a,dia} \right) \quad , \tag{3}$$

$$\left\langle \vec{B} \cdot \vec{u}_a \right\rangle \Big/ B_{ref} = c_{par} u_{a,pol} + c_{per} \left(u_{ExB} + u_{a,dia} \right) \quad , \tag{4}$$

where $c_{per} = \left\langle R^2 \vec{\nabla}\varphi \cdot \vec{B} \right\rangle \Big/ \left(R_{ref} B_{ref} \right)$, $c_{par} = \left\langle B^2 \right\rangle \Big/ B_{ref}^2$, $c_{tor} = \left\langle R^2 \right\rangle \Big/ R_{ref}^2$, $u_{a,pol} = B_{ref} K_a$, $u_{ExB} = R_{ref} \vec{\nabla}\varphi \cdot \vec{E} \times \vec{B} / B^2$, $u_{a,dia} = -\left(R_{ref} / e_a n_a \right) \vec{\nabla}\varphi \cdot \vec{\nabla} P_a \times \vec{B} / B^2$, $u_{ExB} + u_{a,dia} = R_{ref} \Omega_a$. The reference magnetic field B_{ref} is the vacuum field at the geometric center of the vacuum chamber at major radius R_{ref} (table 1). There are three mean field velocities for the main ions $\left(u_{i,pol}, u_{ExB}, u_{i,dia}\right)$. The diamagnetic velocity is determined by particle and energy transport. The ExB velocity is the same for all species. The total parallel and toroidal momentum transport equations [equations (1,2)] solve for the ExB velocity and a poloidal velocity common to all species [14]. The neoclassical equations are used to compute all of the poloidal velocity *differences* that contribute to the collision operator. For a pure plasma, this is just the poloidal (bootstrap) current. This is the minimal modification of neoclassical theory due to turbulence [13]. Note that $u_{i,pol}$ is related to the vertical velocity $v_{i,z}$ that is usually the measured "poloidal" velocity by $v_{i,z} = \vec{u}_i \cdot \vec{\nabla} Z = u_{i,pol} B_z / B_{ref}$. Charge exchange recombination spectroscopy [6] can measure the mean poloidal velocity. The turbulence based methods [16–18] measure the time averaged Doppler shifted phase velocity of the turbulence. Only the mean ExB toroidal velocity contributes to these measurements even if the measurement is of the time delay in the poloidal direction [17,18]. The mean poloidal velocity is parallel to the magnetic field and hence contributes very little to the Doppler shift due to the small parallel wavenumbers of the gyrokinetic turbulence compared to the perpendicular wavenumbers. The ExB velocity that is measured by the Doppler shifted phase velocity is $v_{ExB} = u_{ExB}\ r/\left(R_{ref} q\right)$. Hence the "u" velocities are approximately toroidal projections and the "v" velocities are approximately perpendicular projections. The poloidal velocity

shear only contributes to the parallel velocity shear in the gyrokinetic equations and this is a destabilizing term [19]. Only the shear in the ExB mean velocity Doppler shift is stabilizing to the turbulence apart from "profile shear" effects that cause radial variations in the eigenmode frequencies [20]. Since the mean ExB velocity is purely toroidal, it also contributes to the destabilizing parallel velocity shear. The mean diamagnetic torodial velocity contributes to the phase velocity of the turbulence through its frequency. It also contributes to the parallel velocity.

3. L/H and LCO Solutions

In order to make analysis of the solutions easier the following simplifications are made. A pure plasma is assumed with a single ion species (suppressed species index). The electron inertia and stress are neglected due to the small electron mass. The ion density (n) and the geometry coefficients are taken to be constant. Radial derivatives of only the velocities are retained. The momentum transport equations [equations (1,2)] are reduced to:

$$\frac{\partial}{\partial t} mn \left[c_{per} u_{pol} + c_{tor} \left(u_{ExB} + u_{dia} \right) \right] + \frac{\partial \Pi_{tor}}{\partial r} = S_{tor} \quad , \tag{5}$$

$$\frac{\partial}{\partial t} mn \left[c_{par} u_{pol} + c_{per} \left(u_{ExB} + u_{dia} \right) \right] + \frac{\partial \Pi_{par}}{\partial r} + mn\nu_{pol} \left(u_{pol} - u_{pol}^{neo} \right) = S_{par} \quad . \tag{6}$$

The neoclassical parallel collisional stress yields the poloidal damping terms in equation (6). The poloidal damping rate $\left(\nu_{pol} = \mu_{11} / m_i n_i\right)$ is determined from the NCLASS [21] code coefficient $\left(\mu_{11}\right)$. The poloidal damping rate ν_{pol} has a complex dependence on the ion-ion collision frequency ν_i [14]. At low collision frequency, in the banana regime, the poloidal damping rate is proportional to collision frequency. At high ν_i, in the Pfirsch-Schluter regime, the poloidal damping rate decreases with collision frequency $\nu_{pol} \propto \omega_t^2 / \nu_i$ where $\omega_t = \sqrt{T_i / m_i} / (Rq)$ is the ion transit frequency. The L-mode reference data (Table I) is in the Pfirsch-Schluter regime $\left(\nu^* = \nu_i \Big/ \left(\omega_t (r/R)^{3/2}\right) = 4.5\right)$ and the poloidal damping rate is decreasing as the separatrix is approached (increasing ν_i).

The most natural two independent velocity variables for the turbulent stresses are parallel and ExB toroidal $\left(u_{par}, u_{ExB}\right)$, where $u_{par} = \left\langle \vec{B} \cdot \vec{u} \right\rangle / c_{per} B_{ref}$. The poloidal velocity is eliminated using $u_{pol} = \left(u_{par} - u_{ExB} - u_{dia}\right) c_{per} / c_{par}$ and $a_{per} = c_{tor} c_{par} / c_{per}^2 - 1$. Motivated by gyrokinetic turbulence results [20] the stresses are taken to have the form:

$$\Pi_{tor}^{turb} = \frac{c_{per}^2}{c_{par}} mn \left\{ -\Phi^2 d_{tor} \frac{\partial}{\partial r} \left(u_{par} - \beta_{tor} u_{ExB} \right) \right\} \quad ,$$

$$\Pi_{par}^{turb} = c_{per} mn \left\{ -\Phi^2 d_{par} \frac{\partial}{\partial r} \left(u_{par} - \beta_{tor} u_{ExB} \right) \right\} \quad . \tag{7}$$

The momentum diffusion coeffients $\left(d_{par}, d_{tor}\right)$ are taken to be constants as are the two coefficients of the stress due to the shear in the ExB velocity Doppler shift $\left(\beta_{par}, \beta_{tor}\right)$.

The contribution due to parallel velocity and up/down symmetry breaking of the flux surfaces and other effects [20] are neglected. The geometry coefficients in equation (7) were chosen to reduce the number of coefficients that appear in the final form of the equations. Gyrokinetic turbulence simulations have shown that the ExB velocity shear causes a shift in the radial wavenumber spectrum of electric potential fluctuations. The normalized peak of the shifted potential spectrum that appears in equation (7) is well modeled by the "spectral shift" model [22] which for a single poloidal wavenumber k_y is

$$\Phi = \frac{\gamma/\gamma_0}{\left[1+0.56\left\langle k_x/k_y\right\rangle^2\right]\left[1+\left(1.15\left\langle k_x/k_y\right\rangle\right)^4\right]} \quad , \tag{8a}$$

$$\left\langle k_x/k_y\right\rangle \cong -0.36\,\gamma_{ExB}/\gamma \quad , \qquad \gamma_{ExB} = -\frac{r}{R_{ref}q}\frac{\partial u_{ExB}}{\partial r} \quad . \tag{8b}$$

The linear growthrate γ is here a representative value for the k_y-spectrum. The linear growthrate at the peak of the potential spectrum is a good choice. This is typically 1/3 smaller than the maximum linear growthrate of the spectrum. The potential is normalized by γ_0. The spectral average radial wavenumber shift $\left\langle k_x/k_y\right\rangle$, induced by the ExB velocity shear has been simplified from its more general form [23]. The coefficients in equation (8) are not adjustable parameters to fit experiment but were determined from the properties of the potential spectrum in gyrokinetic turbulence simulations [22].

The collisional contributions to the perpendicular stresses are:

$$\Pi^{col}_{tor} = \frac{c^2_{per}}{c_{par}} mn\left\{-d_{neo}\frac{\partial}{\partial r}\left[u_{par} + a_{per}\left(u_{ExB} + u_{dia}\right)\right]\right\} \quad , \; \Pi^{col}_{par} = c_{per} mn\left\{-d_{neo}\frac{\partial u_{par}}{\partial r}\right\} \quad . \tag{9}$$

The turbulent coefficients $\left(d_{tor}, d_{par}\right)$ are typically two orders of magnitude larger than the Coulomb one d_{neo} [24].

The equations are further reduced to a local flux surface r_s by expanding the three mean velocites: $u_{ExB} = \hat{u}_{ExB}(t)h(r)$, $u_{par} = \hat{u}_{par}(t)h(r)$, $u_{dia} = \hat{u}_{dia}(t)h(r)$. A common radial profile function is assumed $h = 1-(r-r_s)/\Delta_r - 0.5(r-r_s)^2/\Delta_r^2$ to reduce the number of free fitting parameters to just the one length Δ_r. The diamagnetic velocity is treated as an external driver and will be ramped linearly in time $\hat{u}_{dia} = \hat{u}_0(1+c_t t)$. The neoclassical ion poloidal velocity is simplified to be proportional to the diamagnetic velocity $u^{neo}_{pol} = c_{neo}u_{dia}$. Substituting the local radial expansion into the momentum transport equations and evaluating the result at the flux surface r_s gives the final local equations that will be solved.

$$\frac{\partial}{\partial t}\left[\hat{u}_{par} + a_{per}\left(\hat{u}_{ExB} + \hat{u}_{dia}\right)\right] - \Phi_1^2 \frac{d_{tor}}{\Delta_r^2}\left[\hat{u}_{par} - \beta_{tor}\hat{u}_{ExB}\right]$$

$$-\frac{d_{neo}}{\Delta_r^2}\left[\hat{u}_{par} + a_{per}\left(\hat{u}_{ExB} + \hat{u}_{dia}\right)\right] = \hat{S}_{tor} \quad , \tag{10}$$

$$\frac{\partial}{\partial t}\hat{u}_{par} - \Phi_1^2 \frac{d_{par}}{\Delta_r^2}\left[\hat{u}_{par} - \beta_{par}\hat{u}_{ExB}\right] - \frac{d_{neo}}{\Delta_r^2}\hat{u}_{par} + \nu_{pol}\left(\hat{u}_{par} - \hat{u}_{ExB} - \left(1 + c_{neo}\right)\hat{u}_{dia}\right) = \hat{S}_{par} \quad , \tag{11}$$

where $m\,n\,\hat{S}_{tor} = S_{tor}\,c_{par}/c_{per}^2$, $m\,n\,\hat{S}_{par} = S_{par}/c_{per}$. The common intensity factor has been modified to $\Phi_1^2 = \Phi^2 + \Delta_r \partial\Phi^2/\partial r$. For the special case of a constant linear growthrate $\gamma = \gamma_0$ this reduces to $\Phi_1^2 = \Phi^2 + \gamma_{ExB}\partial\Phi^2/\partial\gamma_{ExB}$. This "intensity slope" function Φ_1^2 and the intensity Φ^2 are plotted in figure 1. The reduction of the intensity with increasing γ_{ExB} causes Φ_1^2 to become negative above a critical value of γ_{ExB}. A negative Φ_1^2 causes the normally dissipative turbulence terms in equations (10) and (11) to become drive terms which is the sole cause of both the L/H and the LCO transitions. It is important that Φ_1^2 is positive for low γ_{ExB} so that there is a stable L-mode equilibrium.

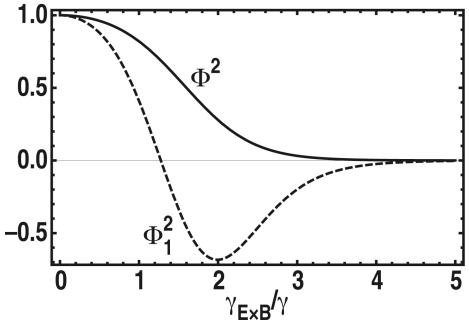

Fig. 1. Spectral shift model [equation (8)] for the peak of the spectrum of electric potential fluctuations Φ^2 (solid) and $\Phi_1^2 = \Phi^2 + \gamma_{ExB}\partial\Phi^2/\partial\gamma_{ExB}$ (dashed) as a function of γ_{ExB}/γ for a constant linear growthrate γ.

Solving the local momentum transport system, without sources, using Mathematica™ gives the particular case with limit cycle oscillations of the 2D momentum transport system shown in figure 2 for the ExB (Doppler phase) velocity (a) The density fluctuation amplitude $\tilde{n}/n = 0.25\Phi$ normalized to the arbitrary unit level of the L-mode measurement in reference [2] (b) and the vertical velocity (c). The parameters of the model were taken from the data as much as possible: $a_{per} = 0.215$, $c_{neo} = 0.2$, $d_{par} = d_{tor} = 10\,m^2/s$, $d_{neo} = 0.01 d_{par}$, $\nu_{pol} = 632/s$. The two coefficients of the Doppler shear pinch, the gradient scale length and the reference linear growth rate were chosen to approximately fit the LCO measurements in figure 4(a,d) of reference [2] at R=2.27 m $\left(\beta_{tor} = 0.1,\ \beta_{par} = 0.17,\ \Delta_r = 0.018\ m,\ \gamma = \gamma_0 = 0.766 \times 10^5\ rad/s\right)$. The dashed line in figure 2(a) is minus the diamagnetic velocity. During the LCO, the ExB velocity is not equal to the diamagnetic velocity but it becomes close to it after the oscillations cease in the H-mode. The neoclassical vertical velocity is shown in figure 2(c) as a dashed line. The simulated vertical velocity settles to the neoclassical value in the H-mode. The LCO frequency given by the model is 1.5 kHz which is a good fit to the observed value of 1.6 kHz. The magnitude of the ExB velocity is well matched. The oscillating poloidal and ExB velocities tend to cancel in the parallel and toroidal velocity but there is a net parallel velocity oscillation during the LCO. The ExB velocitity shear rate is just the ExB velocity [figure 2(a)] divided by the constant

gradient scale length Δ_r and is about a factor of 2 lower than the measured value. The fitting of the model to the data is quite constrained but not unique. The gradient scale length can be reduced to better fit the ExB velocity shear but then the LCO frequency is reduced. The LCO frequency can still be matched by reducing the coefficient β_{par}. However, the maximum vertical velocity during the LCO then increases and it is already too large. The case in figure 2 is a compromise.

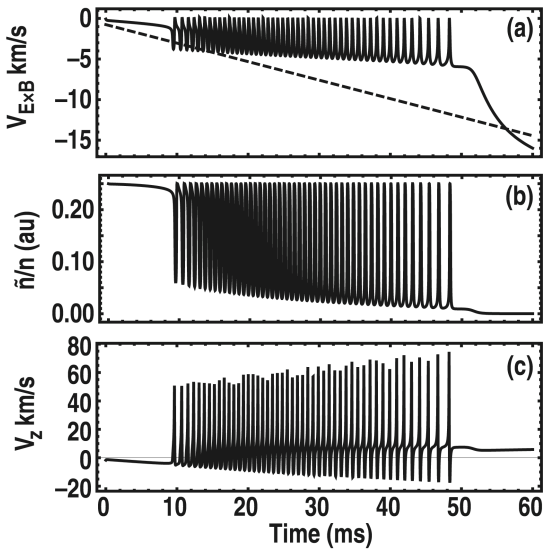

Fig. 2. Time history of the ExB velocity (a) relative density fluctuation amplitude (b) and vertical velocity (c) for an LCO case with constant growth rate.

Scanning only the poloidal damping rate shows that the frequency of the LCO goes up linearly with increasing poloidal damping rate as shown in figure 3. This qualitatively agrees with the trend in the DIII-D data that shows the LCO frequency increases with decreasing density (recall the poloidal damping rate scales inversely with the ion-ion collision rate which increases with density). The line average density of the reference discharge was $\bar{n}_{ref} = 2.65\times10^{19}/m^3$. Using the poloidal damping rate to scale the line average density gives $\bar{n} = \bar{n}_{ref} 632/\nu_{pol}$. The value of the diamagnetic velocity is a proxy for the heating power. The critical value of the diamagnetic velocity at the onset of the LCO and the value required to lock in the H-mode is shown as a function of the scaled line average density in figure 4. This is qualitatively similar to the dependence of the H-mode power threshold (diamagnetic velocity at H-mode) on the line average density with both a linear rise in the power threshold with density above the minimum and a strong increase in the power threshold at low density [16]. All of the other parameters were held fixed in the poloidal damping rate scan. The LCO frequency also depends on the diffusion rate d_{par}/Δ_r^2 and the difference of the Doppler shear coefficients $(\beta_{par} - \beta_{tor})$ in a linear way. This gives a measure of the sensitivity of the results to errors in the date used to constrain the model. The high-density increase of the L/H threshold in figure 4 is caused by the decoupling of the

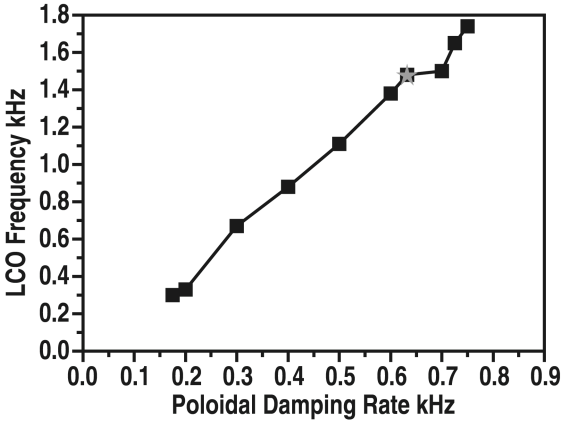

Fig. 3. Variation of the LCO frequency with poloidal damping rate about the reference data point (grey star).

L-mode ExB velocity from the diamagnetic velocity at low poloidal damping rate. The reduction of the L/H threshold with decreasing density carriers onto the LCO threshold curve in figure 4 but the L/H threshold rises sharply below a minimum. This sharp rise in the L/H threshold is due to the ExB velocity being prevented from growing enough to reach the H-mode by the LCO as explained in the next section.

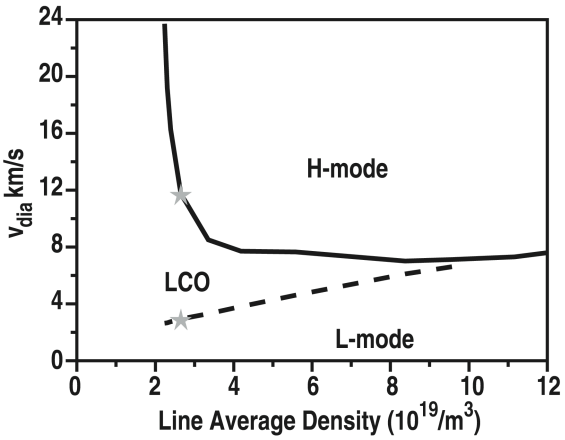

Fig. 4. Critical value of the diamagnetic velocity to trigger and LCO phase (dashed) or an L/H transition (solid) vs line average density scaled from reference data point (grey stars).

The large vertical velocity excursion during the LCO [figure 2(c)] can be reduced by allowing the parallel and ExB velocity gradients lengths to differ. It can also be reduced by including the linear growth rate dependence upon the parallel velocity shear: $\gamma = \gamma_0 + \alpha_{KH} 0.08 \left|\partial u_{par}/\partial r\right|$. This is a physical effect in gyrokinetic theory [19] (Kelvin Helmoltz type mode). The coefficient 0.08 is determined from the GA standard case [20] but a fitting parameter α_{KH} is included. Using the more physical growthrate in the spectral shift model gives a rapid LCO (2.2 kHz) that decays to a quiet phase followed by an L/H transition. This three-stage transition is not seen in the data. In order to get back the two-stage transition adjustments were made $\left(\beta_{par} = 0.24, \gamma_0 = 0.38 \times 10^5 \text{ rad/s}, \alpha_{KH} = 0.11\right)$. The ramp rate of the diamagnetic velocity was also reduced. The resulting waveforms are shown in figure 5. The parallel velocity shear KH drive suppresses the large excursion of the vertical velocity in figure 5(c) so it is now in the observed range for the main ions [25]. The LCO in figure 5 has a lower frequency than the data (0.5 kHz). This model demonstrates that the vertical velocity can be brought into the experimental range by additional physics. This model also introduces a phase shift between the density fluctuation amplitude and the ExB velocity shear as shown in figure 6. Comparing figure 6 to reference [2] figure 3(a,b) it is clear that the density fluctuation amplitude is rising at the time of maximum ExB velocity shear so the counter clockwise rotation of this LCO cycle agrees with the direction measured at this location. It can be shown in general, for the spectral shift model, that if the linear growth rate γ is

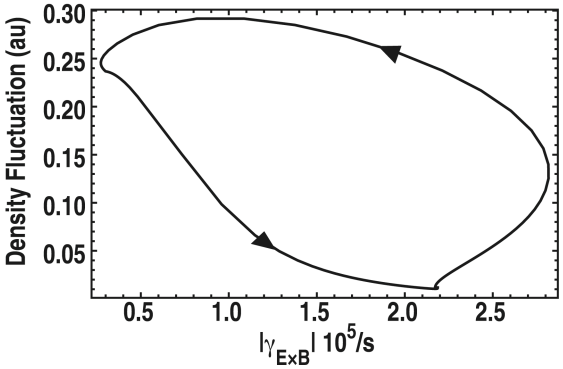

Fig. 5. Time history of the ExB velocity (a) relative density fluctuation amplitude (b) and vertical velocity (c) for the LCO case with KH drive.

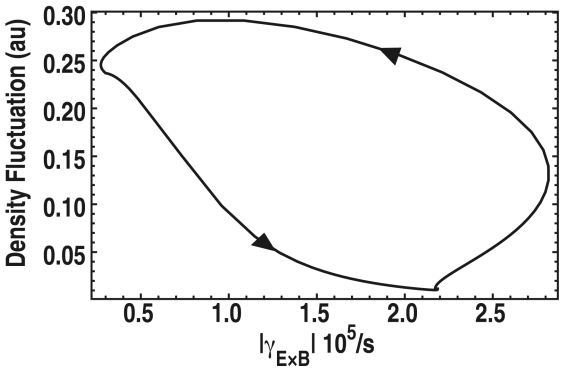

Fig. 6. Relative density fluctuation amplitude vs $|\gamma_{ExB}|$ for the LCO orbit from 202-205 ms in figure 5.

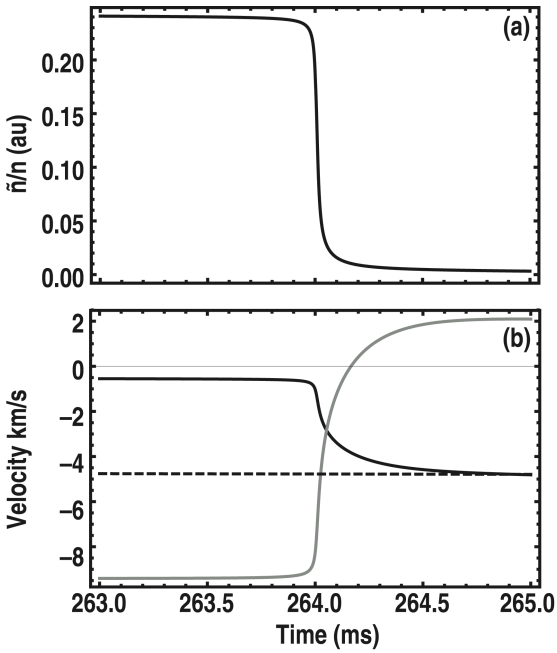

Fig. 7. L/H transition relative density fluctuation amplitude (a) and ExB (black), vertical (grey) and minus the diamagnetic (dashed) velocities (b) vs time (ms).

rising at the peak in the magnitude of the ExB shear, there is a counter clockwise orbit, but if the linear growth rate is falling at the peak in the ExB shear magnitude, the orbit is clockwise. A reduction of the linear growth rate could occur due to a greater steepening of the density gradient than the temperature gradient causing a reduction in the ion temperature gradient mode growthrate. Both directions of the phase orbit are observed in experiments [16].

A one-step L/H transition occurs in the model with KH drive for a smaller gradient scale length $\left(\Delta_r = 0.0154 \text{ m}\right)$ as shown in figure 7. The density fluctuations [figure 7(a)] drop within 0.1 ms and the ExB (black) and vertical (grey) velocities [figure 7(b)] re-arrange within 0.5 ms at the transition. These are the same timescales that have been observed for the "trigger" event at the start of the L/H transition [6]. This fast change in velocity has been called a trigger because it precedes the slower change in the diamagnetic velocity. This is also the case in figure 7(b) since the diamagnetic velocity (dashed) is being ramped at a slow rate.

4. Origin of the Momentum Transport LCO

The origin of the LCO type transition can be understood by examination of the acceleration of the parallel and ExB velocities. The local momentum transport equations [equations (10) and (11)] can be re-written in the following way by diagonalizing the time derivatives and re-grouping terms.

$$a_{per}\frac{\partial \hat{u}_{ExB}}{\partial t} = A_{11}\hat{u}_{ExB} + A_{12}\hat{u}_{par} + s^{ext}_{ExB} \quad , \tag{12a}$$

$$\frac{\partial \hat{u}_{par}}{\partial t} = A_{22}\hat{u}_{par} + A_{21}\hat{u}_{ExB} + s^{ext}_{par} \quad , \tag{12b}$$

The acceleration matrix has the elements:

$$A_{11} = -\Phi_1^2\frac{d_{par}\beta_{par} - d_{tor}\beta_{tor}}{\Delta_r^2} - a_{per}\frac{d_{neo}}{\Delta_r^2} - \nu_{pol} \quad , \qquad A_{22} = -\Phi_1^2\frac{d_{par}}{\Delta_r^2} - \frac{d_{neo}}{\Delta_r^2} - \nu_{pol} \quad , \tag{13a}$$

$$A_{12} = \Phi_1^2\frac{d_{par} - d_{tor}}{\Delta_r^2} + \nu_{pol} \quad , \qquad A_{21} = \Phi_1^2\frac{\beta_{par}d_{par}}{\Delta_r^2} + \nu_{pol} \quad . \tag{13b}$$

And the external sources including the diamagnetic velocity terms are collected into

$$s^{ext}_{ExB} = \hat{S}_{tor} - \hat{S}_{par} - \left[a_{per}\left(\frac{\partial}{\partial t} + \frac{d_{neo}}{\Delta_r^2}\right) + \nu_{pol}\left(1 + c_{neo}\right)\right]\hat{u}_{dia} \quad , \tag{14a}$$

$$s^{ext}_{par} = \hat{S}_{par} + \nu_{pol}\left(1 + c_{neo}\right)\hat{u}_{dia} \quad . \tag{14b}$$

When the intensity slope is positive $\Phi_1^2 > 0$ the acceleration matrix has negative diagonal terms and causes a de-acceleration (decay) of the velocities. For sufficient ExB velocity shear, the intensity slope is negative $\Phi_1^2 < 0$ (figure 1). Assuming both diagonal elements become positive for some value of the ExB velocity shear, the parallel velocity will have a larger diagonal acceleration (A_{22}) than the ExB velocity (A_{11}) since the parallel momentum diffusion is larger than the ExB effective diffusion: $d_{par} > d_{par}\beta_{par} - \beta_{tor}d_{tor}$. There will also be a range of ExB velocity shear where only the parallel diagonal element A_{22} has changed sign causing a growth in parallel velocity and an increase in the turbulence. The off diagonal elements play a critical role in the LCO. If the off-diagonal element in the ExB velocity equation A_{12} is positive, then when the parallel velocity has the opposite sign of the ExB velocity, the off-diagonal term causes a de-acceleration of the ExB velocity. The evolution of the parallel and ExB velocities are plotted in figure 8 for a single LCO cycle (a) and for a single step L/H transition (b) over a 3 ms time frame. Both cases start with a rapid growth of the velocities. The difference between the LCO

and L/H cases is that for the L/H cases the ExB velocity reaches a larger amplitude and the parallel velocity decays due to the elimination of the turbulence drive. For the LCO, the parallel velocity continues to grow in amplitude until it becomes large enough to cause a decay of the ExB velocity and a return to the high turbulence L-mode state. The off-diagonal coupling between velocities is responsible for this. The strong rise in parallel velocity at the end of each LCO cycle has a short duration that makes it difficult to measure with CER but is a signature feature of the LCO predicted by this model. If the parallel and ExB velocities could be made to have the same sign, then the LCO would not occur because the off-diagonal coupling would enhance rather than retard the growth of the ExB velocity resulting in an L/H transition.

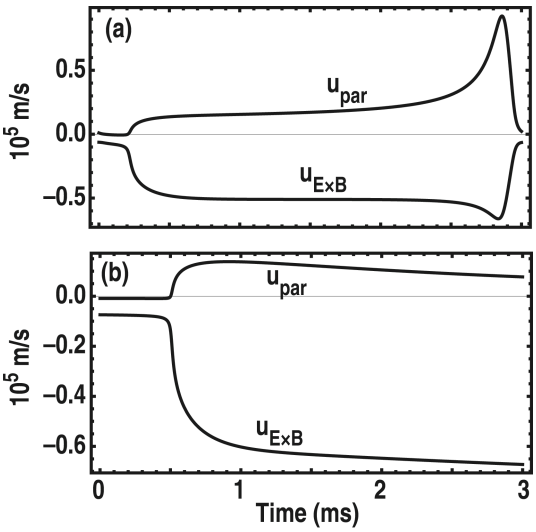

Fig. 8. Parallel velocity u_{par} (positive), ExB velocity u_{ExB} (negative) for a single LCO cycle (a) and for a single step L/H transition (b) over a 3 ms time window.

5. Summary

In this paper it has been shown that the mean field parallel and toroidal momentum equations can have both one-step transitions to suppressed turbulence (L/H) and limit cycle oscillations of the parallel and ExB velocities. Using data from a DIII-D L-mode discharge, it was shown that a simplified model, with the turbulent momentum transport constrained by the power balance diffusivities and the computed neoclassical poloidal damping rate, can fit the LCO frequency, the ExB velocity and the density fluctuation amplitude waveforms in reasonable agreement with the measurements. It was further shown that the frequency scales linearly with the neoclassical poloidal damping rate and that the density dependence of the L/H power threshold is well represented by the model. The counter clockwise phase shift between the density fluctuations and the ExB velocity shear observed in the data is explained by the model as being due to the parallel velocity shear drive of the linear growth rate. The LCO of the momentum equations occurs because there is a weaker growth of the ExB velocity shear than the parallel velocity shear amplitudes. For a high poloidal velocity damping rate, the ExB velocity shear cannot make a full transition to suppressed turbulence and the parallel velocity shear growth de-accelerates the ExB velocity forcing a return to L-mode at the end of the LCO cycle. For weaker poloidal velocity damping, the ExB shear can complete the transition to H mode before the parallel flow grows to a critical level for the LCO. The goal of this work was to establish that the mean field momentum equations can fit the measurements. The next goal is to show that a calibrated quasilinear model of the turbulence, like TGLF [26], can predict the L/H transition and LCO properties without adjustable parameters. There are still many obstacles along the path to a realistic theoretical prediction of the L/H transition including all of the transport channels. This paper has taken the step of verifying that the mean field momentum transport equations capture the non-linear dynamics between the turbulence and the evolution of the mean velocities well enough to reproduce the observed phenomenology of LCO and L/H transitions.

References

[1] Luxon J L *et al* 1986 Plasma Phys. Control. Nucl. Fusion Research (International Atomic Energy Agency, Vienna, 1987), Vol. I, p. 159
[2] Schmitz L *et al* 2012 *Phys. Rev. Lett.* **108** 155002
[3] Staebler G M *et al* 2001 *Nucl. Fusion* **41** 891
[4] Newman D *et al* 1999 *Phys. Plasmas* **6** 854
[5] Burrell K H 1997 *Phys. Plasmas* **4** 1499
[6] Burrell K H *et al* 1996 *Plasma Phys. Control. Fusion* **38** 1313
[7] Shaing K C and Crume Jr E C 1989 *Phys. Rev. Lett.* **63** 2369
[8] Tendler M and Rozhansky V 1990 Controlled Fusion and Plasma Heating, *Proc. of 17th Euro. Conf., Amsterdam* (European Physical Society, Petit-Lancy, Switzerland) Vol. **14B**, p. 744
[9] Frieman E A and Chen L 1982 *Phys. Fluids* **25** 502
[10] Doyle E J *et al* 1991 *Phys. Fluids* **B3** 2300
[11] Shaing K C 1988 *Phys. Fluids* **31** 2249
[12] Sugama H and Horton W 1997 *Phys. Plasmas* **4** 405
[13] Staebler G M 2004 *Phys. Plasmas* **11** 1064
[14] Hirshman S P 1978 *Phys. Fluids* **21** 224
[15] Rozhansky V and Tendler M 1992 *Phys. Fluids* **B4** 1877
[16] Conway G D *et al* 2011 *Phys. Rev. Lett.* **106** 065001
[17] Xu G S *et al* 2011 *Phys. Rev. Lett.* **107** 125001
[18] Yan Z *et al* 2014 *Phys. Rev. Lett.* **112** 125002
[19] Catto P, Rosenbluth M N and Liu C S 1973 *Phys. Fluids* **16** 1719
[20] Waltz R E *et al* 2007 *Phys. Plasmas* **14** 122507
[21] Houlberg W *et al* 1997 *Phys. Plasmas* **4** 3230
[22] Staebler G M *et al* 2013 *Phys. Rev. Lett.* **110** 055003
[23] Staebler G M *et al* 2013 *Nucl. Fusion* **53**, 113017
[24] Hinton F L and Wong S K 1985 *Phys. Fluids* **28** 3082
[25] Kim J C *et al* 1994 *Plasma Phys. Control. Fusion* **36** A183
[26] Staebler G M *et al* 2005 *Phys. Plasmas* **12** 102508

Acknowledgments

This material is based upon work supported by the U.S. Department of Energy, Office of Science, Office of Fusion Energy Sciences, Theory Program, using the DIII-D National Fusion Facility, a DOE Office of Science user facility, under Awards DE-FG02-95ER54309 and DE-FC02-04ER54698.